Manufacturing Rev. **8**, 11 (2021)

https://doi.org/10.1051/mfreview/2021009

Manufacturing Review
Available online at:
https://mfr.edp-open.org

RESEARCH ARTICLE OPEN ACCESS

Simulation of dynamic recrystallization of a magnesium alloy with a cellular automaton method coupled with adaptive activation energy and matrix deformation topology

Sibing Wang, Wenchen Xu*, He Wu, Ranxu Yuan, Xueze Jin, and Debin Shan*

School of Materials Science and Engineering & National Key Laboratory for Precision Hot Processing of Metals, Harbin Institute of Technology, Harbin 150001, China

Received: 11 December 2020 / Accepted: 1 March 2021

Abstract. The cellular automata (CA) model combining topological deformation and adaptive activation energy was successfully constructed to analyze the thermal dynamic recrystallization of the magnesium alloy (AZ61). The simulation datum shown that the recrystallization nucleation located on the grain boundary (GB) once the density of dislocation accumulated to specific value, and the result presents a typical characteristics i.e., repeated nucleation and growth. The simulation results agree well with the experimental results because the activation energy affects recrystallization by affecting nucleation rate.

Keywords: AZ61 magnesium alloy / cellular automaton / adaptive activation energy / deformation topology / dynamic growth criterion

1 Introduction

With increased demands for reducing structure weight as well as reducing energy consumption in aviation and automobile industries, magnesium (Mg) alloys are attracting increased attention due to their excellent properties such as lightweight and high specific strength [1–4]. While these structural components are achieved largely through using forming processes, study of Mg alloys thermal deformation behavior and microstructure evolution is a prerequisite for ensuring to produce high-performance workpieces of Mg alloys.

Bajargan et al. [5] and Xu et al. [6] studied The hot deformation behavior of AZ31/AZ61 Mg alloy, respectively. Recently, Kugler and Turk [7] established the recrystallization kinetics model of isothermal compression, and analyzed the relationship between the average grain size and dynamic recrystallization (DRX) process. Zhang et al. [8], Guo and Ding [9] and Turk and Kugler [10] studied the DRX process by two-dimensional CA model.

In the research reported in this paper, the focus was on the coupling effects of adaptive activation energy and matrix deformation topology on the DRX behavior of magnesium alloys.

2 Materials and methods

The experimental material for hot compression is commercial Mg alloy hot extruded bars (diameter 10 mm, length 500 mm) with nominal composition Mg-5.7Al-0.9Zn-0.5Mn (wt%). Before hot compression, the extruded-rods were heated to 400 °C and held for 4 h to obtain homogeneous microstructure (air cooling). The radius/height of the hot compression samples was 4/12 mm. All the tests of isothermal compression were performed on the thermal simulation testing machine (type: Gleeble-1500D). The range of temperature, strain rate and height reduction was 350–450 °C, 0.001–1 s^{-1} and 0–50%, respectively. The compression procedure is shown in Figure 1. In order to improve the temperature uniformity, the samples were held for 3 minutes before compression.

Each sample was cut along the axial section of the quenched specimens, and then mechanically polished and chemically etched for microstructure analysis. The etchant consisted of picric and acetic acid (27.5 g and 25 ml), distilled water and alcohol (50 and 450 ml). Microstructure results were detected by Olympus-GX71 optical microscope (OM) and Talos F200X transmission electron microscope (TEM). Mean grain size of initial hot compression specimens was 44.6 μm measured by quantitative metallographic method. The specific locations of microstructure simulations and experimental observations are in the central part of the samples.

* e-mail: xuwc_76@hit.edu.cn; shandebin@hit.edu.cn

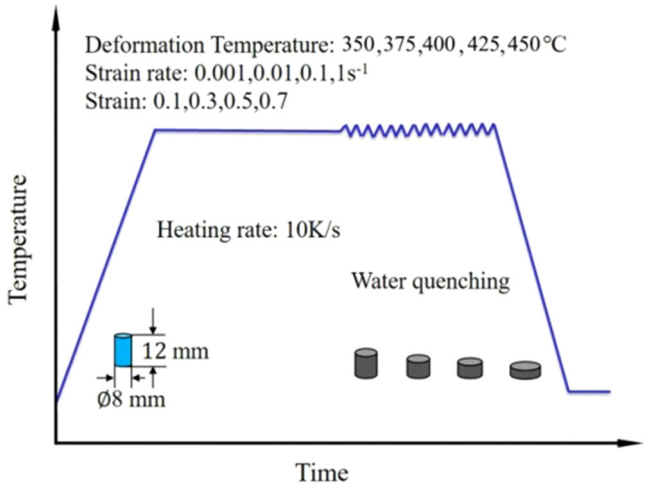

Fig. 1. Experimental procedure for hot compression test.

3 CA models for dynamic recrystallization

3.1 Theoretical model

3.1.1 Modelling for dislocation evolution

The change of dislocation density ρ, with strain ε in the Kocks and Mecking model (K-M model) can be described by [9]:

$$\frac{d\rho}{d\varepsilon} = k_1\sqrt{\rho} - k_2\rho \tag{1}$$

where k_1/k_2 represents the hardening /dynamic softening parameter.

Based on the shear modulus G and the Burgers vector b, the flow stress σ can be calculated by [9]:

$$\sigma = \alpha' Gb\sqrt{\rho} \tag{2}$$

where the value of the interaction factor α' is 0.5–1.0. Based on N, the number of the total cells, and ρ_i, the mean ρ of all cells', $\overline{\rho}$, could be given by:

$$\overline{\rho} = \frac{1}{N}\sum_{i=1}^{n}\rho_i \tag{3}$$

3.1.2 Modelling for DRX nucleation and growth

Based on the strain rate $\dot{\varepsilon}$, temperature T and the universal gas constant R, the dynamic recrystallization nucleation rate could be given by [9]:

$$\dot{n}(\dot{\varepsilon}, T) = C\dot{\varepsilon}^m \exp\left(-\frac{Q_{act}}{RT}\right) \tag{4}$$

where C represents a constant determined by an inverse analysis method, and m denotes a strain rate sensitive exponent, which is usually set as 1.0 in the CA simulation according to Refs. [11–14]. The deformation activation energy Q_{act} could be calculated by the result of hot compression experiments [15]. The nucleation rate $\dot{n}$ can be inversely calculated by the following expression [10]:

$$\eta = \dot{n}\frac{\varepsilon}{\dot{\varepsilon}}\frac{4}{3}\pi r_d^3 \tag{5}$$

where r_{d} represents the mean radius of the recrystallized grains, and η is the DRX percentage of experimentally result. The critical ρ of DRX during hot deformation could be calculated by [9].

$$\rho_c = \left(\frac{20\gamma\dot{\varepsilon}}{3blM\tau^2}\right)^{1/3} \tag{6}$$

where the symbol τ represents the line energy of dislocation, and symbol γ means the energy of grain boundary (GB), see equations (7) [8] and (8) [9]. The dislocation mean free path l and the mobility ratio M of GB was expressed by equations (9)–(11).

$$\gamma_i = \begin{cases} \gamma_m & \theta_i \geq 15^\circ \\ \gamma_i = \gamma_m\dfrac{\theta_i}{\theta_m}\left(1 - \ln\left(\dfrac{\theta_i}{\theta_m}\right)\right) & \theta_i < 15^\circ \end{cases} \tag{7}$$

where the θ_{i} represents the i_{th} recrystallized grain misorientation with its neighboring one, and θ_{m} means the high angle misorientation (taken as 15°).

$$\gamma_m = \frac{Gb\theta_m}{4\pi(1-\mu)} \tag{8}$$

where μ is the Poisson's ratio.

$$l = \frac{K_1 Gb}{\sigma} \tag{9}$$

where the constant K_1 is usually about 10 for most metals.

$$M = \frac{\delta D_{ob} b}{KT}\exp\left(\frac{-Q_b}{RT}\right) \tag{10}$$

where K represents Boltzmann's constant. The δ, Q_{b} and D_{ob} are the characteristic grain boundary thickness, diffusion activation energy and diffusion factor, respectively.

3.1.3 Modelling of DRX growing

The driving force (Δf_{i}) depends on the difference of ρ_{m} and ρ_{d} [10]:

$$v_i = M\Delta f_i \tag{11}$$

For the assumed spherical recrystallized grains:

$$\Delta f_i = \tau(\rho_m - \rho_d) - \frac{2\gamma}{r_i} \tag{12}$$

where r_{i} and $\rho_{\mathrm{d}}/\rho_{\mathrm{m}}$ is the radius and ρ of recrystallized grain / matrix, respectively.

Displacement increment (Δx_{i}) and time increment (Δt) could be calculated by equations (13) and (14):

$$\Delta x_i = v_i \Delta t \tag{13}$$

$$\Delta t = \frac{L_0}{V_{\max}} = \frac{k_2^2 L_0}{M\tau k_1^2} \tag{14}$$

In this study, the length and width of each cell are both set as the constant L_0 in the hot compression process, the growth criterion can be written as:

$$\Delta x_i > L_0\left(\sqrt{\frac{n_i+1}{\pi}} - \sqrt{\frac{n_i}{\pi}}\right) \tag{15}$$

where n_{i} denotes the number of cells in the i_{th} DRX grain.

3.2 Simulation conditions of solution-treated (ST) and as-rolled (AR) alloy

In this study, the total cell number is 160 000 (initial matrix size 400×400) in the CA model, which corresponds to $1000\,\mu\mathrm{m} \times 1000\,\mu\mathrm{m}$ in a real sample. The length and width L_0 of each cell is arbitrarily chosen to be $2.5\,\mu\mathrm{m}$. Meanwhile, the Neumann's neighboring rule and periodic boundary conditions are applied in this CA simulation.

3.3 General model for matrix deformation

3.3.1 Matrix deformation theory

In this work, the grain shape is supposed to be spherical, which changes into an ellipsoid during the compression process. The deformation is described by the 2×2 matrix, thus the homogenous deformation matrix S can convert the vector u into v as follows:

$$v = Su \tag{16}$$

Based on the initial vector (u_i (where, $i = x,y$)), new vector (v_i (where, $i = x,y$)) and principle nominal deformation in x and y direction (l_i (where, $i = x,y$)), the matrix can be written as:

$$\begin{bmatrix} v_x \\ v_y \end{bmatrix} = \begin{bmatrix} l_x & 0 \\ 0 & l_y \end{bmatrix} \begin{bmatrix} u_x \\ u_y \end{bmatrix} \tag{17}$$

where l_{i} denotes the ratio of final length to the original length of the unit vector ahead the axes, and $l_x l_y = 1$.

3.3.2 Matrix deformation model

The dimensions of initial matrix and deformed matrix are supposed to be a × b and $m \times n$, respectively. Assuming that the area in 2D model remain constant during deformation, $a \times b = m \times n$. In the MATLAB model, LCA represents the length of each square cell. The initial matrix height is $a \times LCA$, and the deformed matrix height is $m \times LCA$, thus the true strain εt and engineering strain ε_e can be described as follows:

$$\varepsilon_t = \left|\ln\frac{m \times L_{CA}}{a \times L_{CA}}\right| = \ln\frac{a}{m} \tag{18}$$

$$\varepsilon_e = \left|\frac{m \times L_{CA} - a \times L_{CA}}{a \times L_{CA}}\right| = \frac{a-m}{a} \tag{19}$$

The relationship between ε_e and ε_t can be obtained by

$$\varepsilon_e = 1 - \exp(-\varepsilon_t) \tag{20}$$

Then the rows m of deformed-matrix can be calculated by

$$m = a \times \exp(-\varepsilon_t) \tag{21}$$

The columns n of deformed-matrix can be calculated by

$$n = a \times b/m \tag{22}$$

3.3.3 Matrix transformation

Figure 2a and b show the example of geometry change between initial and deformed grain due to matrix deformation in the compression process. It can be seen that there are 20 surrounding neighbors (shown in white dot) of the initial grain (green color), which increases to 22 neighbors after compression deformation, thus the DRX nucleation sites should become more. Therefore, in order to model the DRX process more accurately, the rule of matrix deformation is adopted in this study.

The coordinate of each cell with given orientation value, O_{ri}, in the initial matrix should be transferred to a new one to match the deformed matrix. Meanwhile, the cells in an identical grain are assigned the same orientation value, O_{ri}, to distinguish different grains, which means that the cells with the same O_{ri} belong to the unique grain, otherwise not. The coordinate transformation could be described in equations (23) and (24):

$$i = \begin{cases} ceil\left[\dfrac{i'}{1-\varepsilon_e}\right], & ceil\left[\dfrac{i'}{1-\varepsilon_e}\right] < a \\ a, & ceil\left[\dfrac{i'}{1-\varepsilon_e}\right] \geq a \end{cases} \tag{23}$$

$$j = \begin{cases} ceil[j' \times (1-\varepsilon_e)], & ceil[j' \times (1-\varepsilon_e)] < b \\ b, & ceil[j' \times (1-\varepsilon_e)] \geq b \end{cases} \tag{24}$$

where Ceil (X) is a numerical method to get a smallest integer not less than X. The variable *i(i')* and *j(j')* represent the initial matrix (deformed matrix) x and y ordinate, respectively. After deformation is finished, the orientation O_{ri} (i, j) of the cell $S_{i,j}$ in the initial matrix S (a, b), i.e. matrix S with a rows and b columns, should be transferred to the cell $S'_{i',\ j'}$ in the deformed matrix S' (m, n), i.e. matrix S' with m rows and n columns.

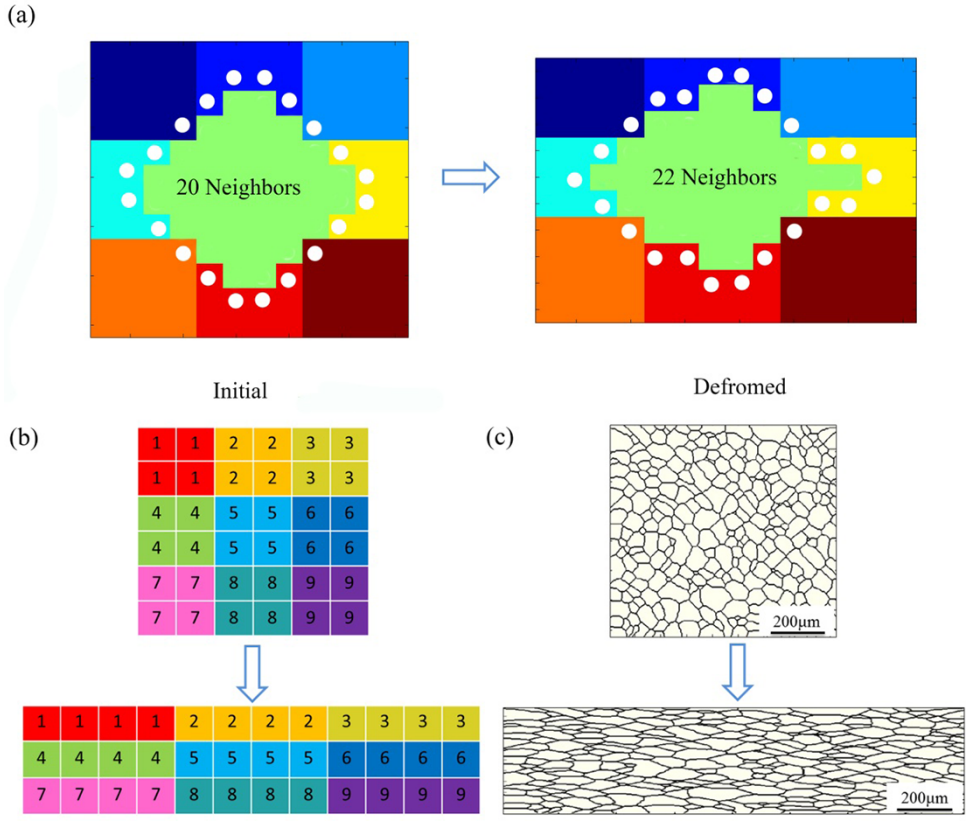

Fig. 2. Schematic diagram of grain topology with matrix deformation: (a) schematic diagram of geometry change due to matrix deformation, (b) schematic diagram of matrix deformation, $\varepsilon_e = 0.5$, (c) grain topology induced by matrix deformation, $\varepsilon_e = 0.5$, (initial average grain size $d_0 = 44.5\ \mu m$).

Figure 2b show the schematic diagrams of matrix deformation and grain topology under certain strain. There are 9 grains with different O_{ri} (1–9) and colors in initial matrix, and each grain has four cells with the same O_{ri}, as illustrated in Figure 2b. As the matrix deformation reaches 50%, the initial two-dimensional matrix S (6, 6) is changed into a new two-dimensional matrix S' (3, 12), and thus the geometry of initial matrix will change correspondingly. Meanwhile, the information of each cell in initial matrix is transferred to the corresponding cell in deformed matrix, respectively. For instance, cell $S'_{2,5}$ corresponds to $S_{4,3}$ and $S'_{2,7}$ corresponds to $S_{4,4}$ according to equations (23) and (24). Figure 2c displays the grains topology caused by matrix deformation with initial average grain size 44.5 μm, which is close to that in the solution treated AZ61 Mg alloy in this study.

4 Results and discussion

4.1 Hot compression strain-stress analysis

Figure 3 presents the experimental results of hot compression with the T of 350–450 °C. As the true strain enhanced, the stress increased dramatically and continuously. Beyond the maximum value, the stress reduced gradually and even to a steady state.

The adaptive activation energy Q_{act} under different true strains ε were incorporated into the CA model. The $Qact$ corresponding to ε varying from 0.05 to 0.7 were calculated with interval of 0.05. Through linear fitting of $\ln\sinh(\alpha\sigma) - 1/T$ and $\ln\sinh(\alpha\sigma) - \ln\varepsilon$, the activation energy Q_{act} was calculated as 166 KJ. Based on the linear relationship of $\ln Z - \ln\sinh(\alpha\sigma)$, where Z is the Zener-Hollomon parameter, the stress constant n of as-received AZ61 Mg alloy was calculated to be 8.7, and the correlation coefficient reached 0.908, which indicates that it was reliable to describe the hot deformation behavior of the Mg alloy by using hyperbolic sine law [1]. By means of least squares polynomial fitting of the deformation energy under various strains, the evolution of deformation energy Q_{act} with true strain can be written as:

$$Q_{act} = 214 - 208\varepsilon + 315\varepsilon^2 - 938\varepsilon^3 + 1651\varepsilon^4 - 905\varepsilon^5 \quad (25)$$

4.2 Microstructural evolution of simulaiton

Figure 4 exhibits the simulation results of microstructure evolution of AZ61 magnesium alloy under hot deformation (400 °C, $\dot{\varepsilon} = 0.001\ s^{-1}$).

4.3 Flow stress prediction using simulation

Figure 5 compares the peak stress and s one of the AZ61 magnesium alloy. There is little difference between the experimental datum and simulated ones.

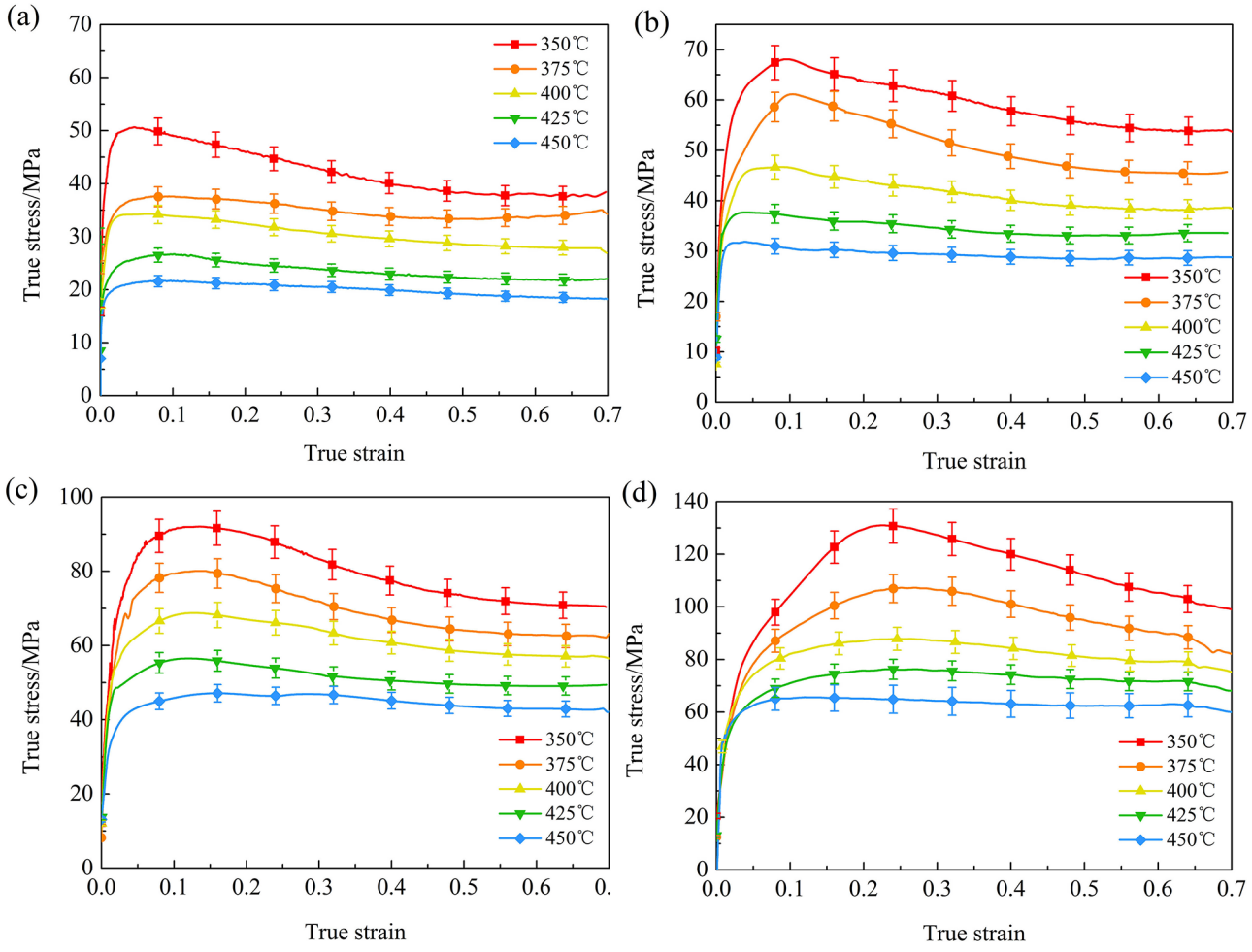

Fig. 3. Hot compression results of AZ61 magnesium alloy: (a) $\dot{\varepsilon} = 0.001\ s^{-1}$; (b) $\dot{\varepsilon} = 0.01\ s^{-1}$; (c) $\dot{\varepsilon} = 0.1\ s^{-1}$; (d) $\dot{\varepsilon} = 1\ s^{-1}$.

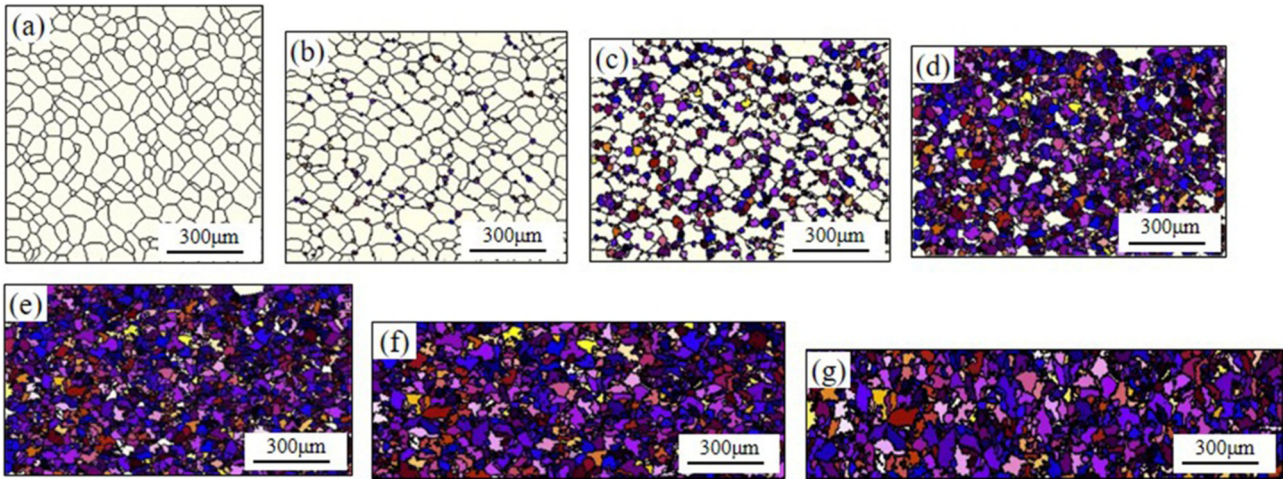

Fig. 4. AZ61 microstructure of simulation result under hot deformation with different ε (400 °C, $\dot{\varepsilon} = 0.001\ s^{-1}$): (a) $\varepsilon_t = 0$, (b) $\varepsilon_t = 0.1$, (c) $\varepsilon_t = 0.15$, (d) $\varepsilon_t = 0.2$, (e) $\varepsilon_t = 0.3$, (f) $\varepsilon_t = 0.5$, (g) $\varepsilon_t = 0.7$.

4.4 Microstructure prediction during hot compression

Figure 6 presents the simulated and experimental microstructures of hot deformation samples under different T. Table 1 lists the average grain sizes of simulated and experimental results.

Figure 7 presents the variation curves of dynamic recrystallization, including volume fraction and average

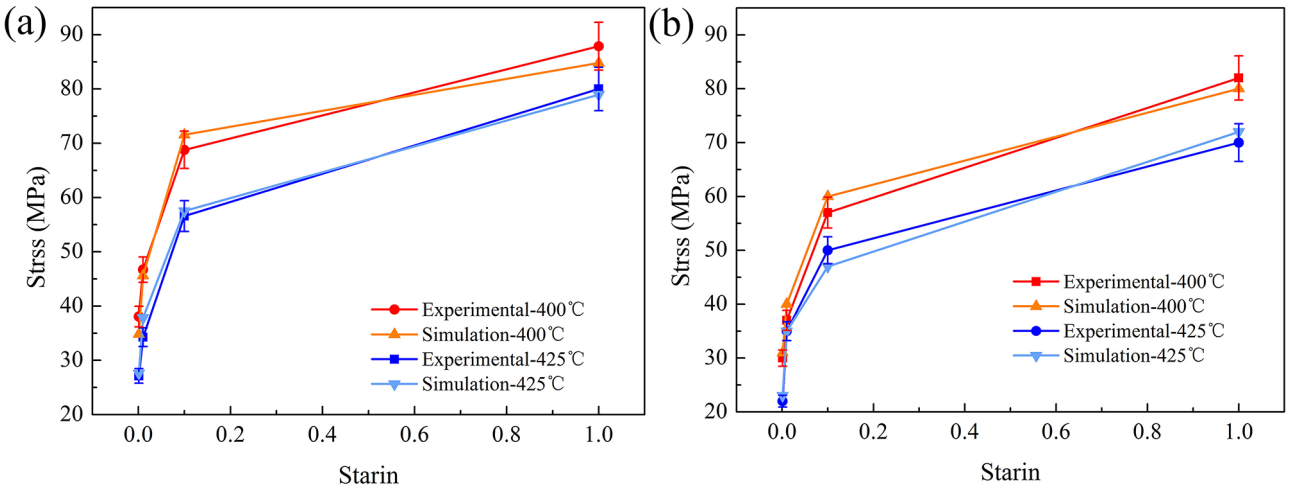

Fig. 5. Comparison between peak stress and steady stress by experimental and simulation of AZ61 magnesium alloy sample ($T = 400$ and 425 °C, $\dot{\varepsilon} = 0.001$–1 s^{-1}): (a) σ_p-strain, (b) steady stress-strain.

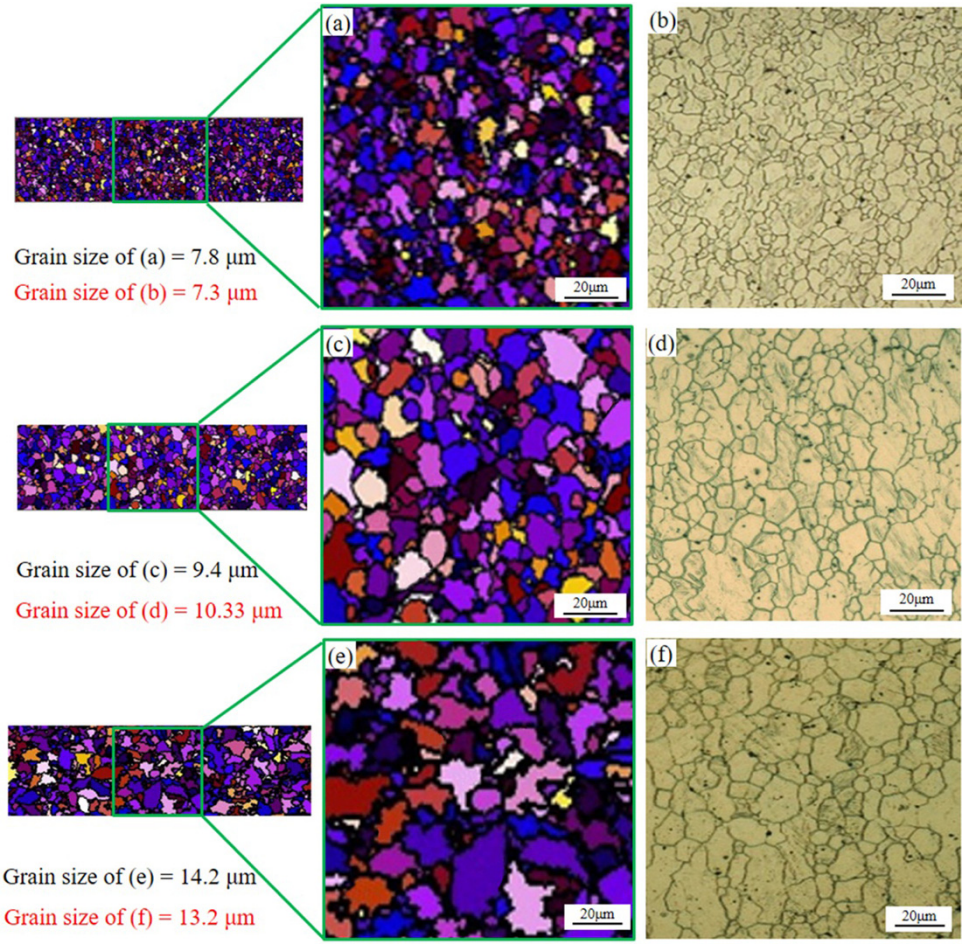

Fig. 6. Microstructures comparison between CA simulation datum and experimental results and different T ($\dot{\varepsilon} = 0.001$ s^{-1}, $\varepsilon = 0.7$): (a) and (b) $T = 350$ °C; (c) and (d) $T = 400$ °C; (e) and (f) $T = 450$ °C.

grain size. When the strain rate increased, the dislocation pile-up was more serious and the dislocation storage energy became greater, resulting in higher DRX nucleation rate and more recrystallized grains. However, the DRX grains did not have enough time to grow up under high strain rate, thus the grain size was smaller under high strain rate than that under low strain rate when the DRX process was completed. Also, it could be found that the mean grain size

Table 1. Average grain size of simulation and experimental results under true strain $\varepsilon = 0.7$.

$T/(°C)$	350	350	400	400	450	450
$\dot{\varepsilon}/(s^{-1})$	0.001	0.1	0.001	0.1	0.001	0.1
Simulation (μm)	7.8	5.0	9.4	7.77	14.2	8.7
Experiment (μm)	7.3 ± 0.4	5.1 ± 0.2	10.33 ± 0.5	7.06 ± 0.3	13.2 ± 0.6	9.2 ± 0.3
Deviation (%)	6.8	1.9	9	10	7.5	5.4

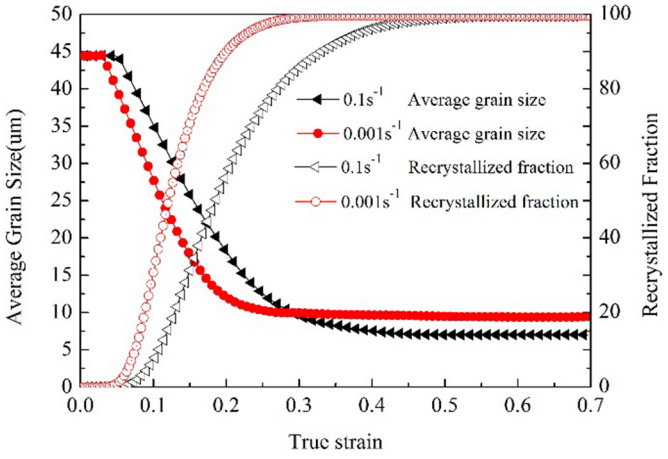

Fig. 7. The relationship between average grain size, strain rate, and recrystallization fraction ($T = 400\,°C$, $\dot{\varepsilon} = 0.1\,s^{-1}$)

reduced once the dynamic recrystallization occurred. With the progress of hot compression, the DRX fraction increased gradually. Until the plastic strain reached certain value, the DRX process finished and then the DRX grains ceased to refine.

5 Conclusions

The CA model coupled with adaptive deformation energy and matrix deformation topology has been established to simulate the DRX process of AZ61 magnesium alloy in the temperature range of 350 ~ 450 °C and the strain rate range of 0.001-1 s-1. The simulated peak stress and steady stress values were very close to the experimental ones. The deviation of the average grain size between the simulation and experimental results was less than 10%.

Meanwhile, the simulated DRX process as well as microstructure evolution was in good accordance with the experimental ones from the hot compression of AZ61 Mg alloy, which indicates the reliability of the present CA model coupled with adaptive activation energy and topology deformation technology.

The CA simulation results indicate that the decrease of strain rate accelerated the DXR process and the mean grain size increased with the decrease of strain rate, which was quite consistent with the experimental results of the hot compression.

Nomenclature

ρ	Dislocation density
ε	True strain
k_1	Hardening parameters
k_2	Softening parameters
Σ	Flow stress
G	Shear modulus
b	Burgers vector
$\overline{\rho}$	Mean dislocation density of all cells
ρ_i	Dislocation density of Number i cell
N	The number of total cells
$\dot{n}$	Nucleation rate
C	Constant
m	Strain rate sensitive exponent, set as 1.0
Q_{act}	Deformation activation energy
R	Universal gas constant, 8.31
T	Deformation temperature
$\dot{\varepsilon}$	Strain rate
A_0	Material constants
n	Material constants
α	Material constants
η	DRX percentage
r_d	Mean radius of recrystallized grains
ρ_c	Critical dislocation density
γ	Grain boundary energy
l	Dislocation mean free path
M	Grain boundary mobility ratio
θ_{i}	grain boundary misorientation
γ_{m}	Grain boundary energy
θ_{i}	Grain boundary misorientation between the i_{th} recrystallized grain and its neighboring grain
θ_{m}	Grain boundary misorientation in the case of the occurrence of a high angle boundary (taken as 15°)
μ	Poisson's ratio
K_1	Constant of 10 for most metals
δ	Characteristic grain boundary thickness
D_{ob}	Boundary self-diffusion coefficient
K	Boltzmann's constant
Q_{b}	Activation energy for the boundary diffusion.
v_{i}	Growth velocity
Δf_{i}	Driving force for the i_{th} recrystallized grain
ρ_m	Dislocation density of the matrix
ρ_d	Dislocation density of recrystallized grain
r_{i}	The radius of the i_{th} recrystallized grain

Δx_{i}	Displacement increment of i_{th} recrystallized grain
Δt	Time increment
L_0	Length of each cell
n_{i}	The numbers of cells in the i_{th} DRX grain
u_i $(i = x,y)$	Initial vector of x and y direction
v_i $(i = x,y)$	New vector of x and y direction after deformation
l_{i} $(i = x,y)$	Length in x, y axes of deformed matrix
ε_e	Engineering strain
ε_t	True strain
$a \times b$	Cell number of row × column (initial matrix)
$m \times n$	Cell number of row × column (deformed matrix)
ceil(x)	map a the smallest integer not less than x
σ_{p}	Peak stress
ε_c	Critical strain
ε_p	Peak strain
k	Material constants
θ	Strain hardening
σ_{ss}	Steady-state stress
X_{DRX}	Dynamic recrystallization fraction

This work is supported by the National Natural Science Foundation of China (No. 51775137).

Author contribution

Wenchen Xu, Writing-Review & Editing; Sibing Wang, Writing-Original Draft Preparation, He Wu, Data curation; Ranxu Yuan, software; Xueze Jin, performed the experiments and Data curation; Debin Shan, Supervision.

References

1. H. Yu, Y. Sun, L. Hu, Z. Wan, H. Zhou, J. Alloys Compd. **704** (2017) 537–544
2. S.-M. Baek, H.J. Kim, H.Y. Jeong, S.-D. Sohn, H.-J. Shin, K.-J. Choi, K.-S. Lee, J.G. Lee, C.D. Yim, B.S. You, H.-Y. Ha, S.S. Park, Corros. Sci. **112** (2016) 44–53
3. O. Hilšer, S. Rusz, P. Szkandera, L. Čížek, M. Kraus, J. Džugan, W. Maziarz, Metals **8** (2018) 776
4. C.-C. Zhang, H.-Y. Wang, M. Zha, C. Wang, J.-H. Li, Z.-Z. Yang, Q.-C. Jiang, Materials **11** (2018) 895
5. G. Bajargan, G. Singh, D. Sivakumar, U. Ramamurty, Mater. Sci. Eng. A **579** (2013) 26–34
6. Y. Xu, L. Hu, Y. Sun, J. Alloys Compd. **580** (2013) 262–269
7. G. Kugler, R. Turk, Comput. Mater. Sci. **37** (2006) 284–291
8. Y. Zhang, S. Jiang, Y. Liang, L. Hu, Comput. Mater. Sci. **71** (2013) 124–134
9. R. Ding, Z.X. Guo, Comput. Mater. Sci. **23** (2002) 209–218
10. G. Kugler, R. Turk, Acta Mater. **52** (2004) 4659–4668
11. H.J. McQueen, N.D. Ryan, Mater. Sci. Eng. A **322** (2002) 43–63
12. R. Ding, Z.X. Guo, Acta Mater. **49** (2001) 3163–3175
13. S. Hore, S.K. Das, S. Banerjee, S. Mukherjee, Mater. Sci. Technol. **28** (2012) 711–718
14. P. Peczak, M.J. Luton, Philos. Mag. **70** (1994) 817–849
15. Z. Jin, Z. Cui, Comput. Mater. Sci. **63** (2012) 249–255

Cite this article as: Sibing Wang, Wenchen Xu, He Wu, Ranxu Yuan, Xueze Jin, Debin Shan, Simulation of dynamic recrystallization of a magnesium alloy with a cellular automaton method coupled with adaptive activation energy and matrix deformation topology, Manufacturing Rev. **8**, 11 (2021)